Science Advances
AAAS

advances.sciencemag.org/cgi/content/full/4/7/eaat1061/DC1

Supplementary Materials for

Domain Meissner state and spontaneous vortex-antivortex generation in the ferromagnetic superconductor $EuFe_2(As_{0.79}P_{0.21})_2$

Vasily S. Stolyarov*, Ivan S. Veshchunov, Sergey Yu. Grebenchuk, Denis S. Baranov, Igor A. Golovchanskiy, Andrey G. Shishkin, Nan Zhou, Zhixiang Shi, Xiaofeng Xu, Sunseng Pyon, Yue Sun, Wenhe Jiao, Guang-Han Cao, Lev Ya. Vinnikov, Alexander A. Golubov, Tsuyoshi Tamegai, Alexander I. Buzdin, Dimitri Roditchev*

*Corresponding author. Email: stoliarov.vs@mipt.ru (V.S.S.); dimitri.roditchev@espci.fr (D.R.)

Published 13 July 2018, *Sci. Adv.* **4**, eaat1061 (2018)
DOI: 10.1126/sciadv.aat1061

The PDF file includes:

Other Supplementary Material for this manuscript includes the following:

(available at advances.sciencemag.org/cgi/content/full/4/7/eaat1061/DC1)

Movie S1 (.mp4 format). Movie of the local V-AV nucleation and domain structure evolution at DMS/DVS.

Section S1. Sample characterizations

Single crystals of $EuFe_2(As_{0.79}P_{0.21})_2$ were grown using the self-flux method (*8*), after stoichiometric amounts of N4 purity starting materials with the nominal composition $x \sim 0.28$ were mixed thoroughly and loaded into an alumina crucible. The crucible was then sealed in a quartz ampoule in vacuum, heated to 1300°C at a rate of 50°C/h and kept at this temperature for 12 h before cooling to 950°C at a cooling rate of 3°C/h. The actual chemical composition of the studied crystal was determined using EDX analysis on Carl Zeiss Supra 50VP scanning electron microscope. The X-ray diffraction performed on the grown crystal showed only (00l) reflections, indicating that the crystallographic c-axis is perpendicular to the crystal plane. From (002) reflection peak the lattice parameter c was calculated to be 11.885 Å, close to the value found in Ref. (*5*) for $EuFe_2(As_{0.79}P_{0.21})_2$ compound.

The electric in-plane (ab-plane) resistivity ρ_{ab} was measured by a standard four-probe method using the Quantum Design physical property measurement system (PPMS). The results of transport measurements are presented in fig. S1(A,B). The sample showed metallic behaviour with ρ_{ab} increasing almost linearly with temperature. The residual resistivity ratio (RRR) is ρ_{ab}(300 K)/ρ_{ab}(27 K)$\simeq$ 5. The value of RRR is similar to those previously reported for optimally P-substituted $EuFe_2(As_{1-x}P_x)_2$ single crystals (*5, 8*). The superconducting critical temperature $T_c = 24.2$ K was determined by 50% resistivity drop in zero applied magnetic field. The magnetic field evolution of $\rho_{ab}(T)$ is presented in fig. S1(B). In these experiments the magnetic field was applied $H \| c$. Note that the forced alignment of Eu^{2+} moments by the external magnetic field causes a clear negative magnetoresistance. At $T \sim$ 17-18 K, which corresponds to the observed DMS/DVS transition (discussed in the main text), the upper critical field, determined under the criterion $\rho(T) = 0.5\rho_n$, i.e. by 50% drop of the normal state resistivity, is $\mu_0 H_{c2}^{//c}(18\ K) \simeq 4$ T. Using the standard relation $\mu_0 H_{c2}^{//c}(T) = \Phi_0/2\pi\xi_{ab}^2(T)$, where $\Phi_0 = 2.068 \times 10^{-15}$ Wb is the magnetic flux quantum, we get an estimate for the superconducting coherence length at the DMS/DVS transition, $\xi_{ab}(18\text{K}) \sim 9.1$ nm.

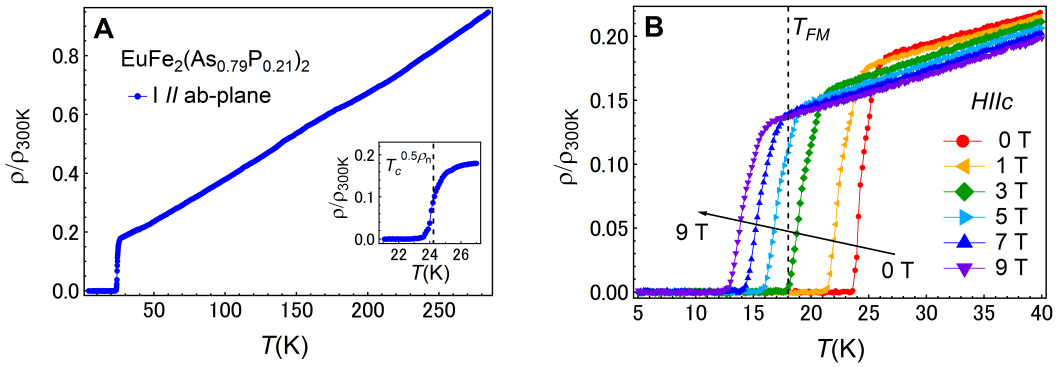

Fig. S1. Resistance temperature dependence.
(A) Temperature dependence of the normalized in-plane (ab-plane) resistivity for $EuFe_2(As_{0.79}P_{0.21})_2$ single crystal. The inset shows sharp ($\Delta T_c \sim 2.4$ K) superconducting drop at $T_c^{\rm onset} \simeq 26$ K. The superconducting critical temperature $T_c = 24.2$ K was determined under the criterion $\rho(T) = 0.5\rho_n$ (by 50% drop of the normal state resistivity). (B) Temperature dependence of the normalized in-plane (ab-plane) resistivity of $EuFe_2(As_{0.79}P_{0.21})_2$ single crystal under different magnetic fields along the c-axis.

The coexistence of ferromagnetism and superconductivity in our $EuFe_2(As_{0.79}P_{0.21})_2$ single crystals was first verified conventionally, employing magnetization measurements at fields up to 5 T, using a commercial Quantum Design MPMS-XL5 SQUID magnetometer. For magnetization measurements the plate-like sample was cut into a $1 \times 1 \times 0.015$ mm^3 rectangle. Zero-field cooled (ZFC) and field-cooled (FC) $M(T)$ magnetization curves of $EuFe_2(As_{0.79}P_{0.21})_2$ are shown in Fig. 1(c) of the main text. In ZFC mode magnetization data were acquired at the warming part of the ZFC cycle. The diamagnetic signal due to superconductivity is revealed below 22 K. Negative susceptibility is not achieved at $T_c^0 = 23.6$ K of the zero resistivity in small applied magnetic field $\sim$ 10 Oe, due to the dominant effect of strong paramagnetism of Eu^{2+} sub-lattice above $T_{FM} \sim 18$ K and tiny amount of ferromagnetic impurity Fe_2P with $T_{FM} \sim 306$ K in these crystals (*5*). Step features in ZFC and FC $M(T)$ magnetization curves near 18 K are attributed to the ferromagnetic phase transition, in agreement with previously reported findings (*5, 6, 32*).

Typical magnetization vs magnetic field $M(H)$ curves acquired at various temperatures are shown in fig. S2(A). The magnetic field was directed parallel to the c-axis of the crystal. The peculiar shape

of the loops can be understood considering a superposition of typical hysteresis loops of a type-II superconductor and the magnetization of Eu^{2+} ferromagnetic subsystem (*6*).

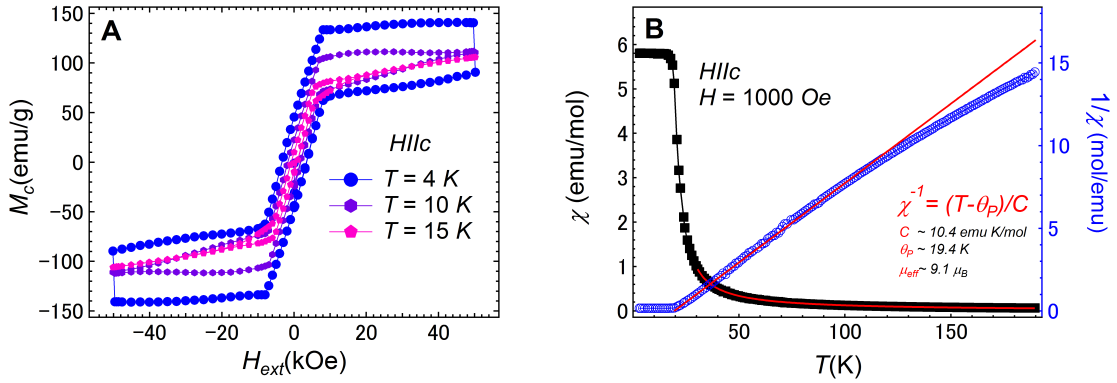

Fig. S2. *M*(*H*) and χ(*T*) curves acquired on $EuFe_2(As_{0.79}P_{0.21})_2$ crystal.
(A) $M(H)$ curves acquired at different temperatures on $EuFe_2(As_{0.79}P_{0.21})_2$ crystal used in MFM experiments. The magnetic field was applied along the c-axis. (B) Temperature dependence of the field-cooled DC-magnetic susceptibility χ and the inverse magnetic susceptibility $1/\chi$ measured at H =1,000 Oe. The fitting results using the Curie-Weiss law, $\chi = C/(T-\theta_P)$, are shown as red line and red curve in the plots of $1/\chi$ and χ, respectively. The paramagnetic Curie temperature (Weiss constant) θ_P is determined by linear extrapolation of the $1/\chi$ vs T plot to $1/\chi = 0$.

Figure S2(B) shows the temperature dependence of the magnetic susceptibility and inverse magnetic susceptibility measured under magnetic field H =1,000 Oe applied along the c-axis for the single crystal $EuFe_2(As_{0.79}P_{0.21})_2$ of approximate dimensions of $1.1\times1.0\times0.11$ mm^3. The fits of the high-temperature tail of the susceptibility data (between 30 and 190 K) using the Curie-Weiss law, $\chi = C/(T-\theta_P)$, yield the Curie-Weiss constant $C = 9.4$ emu·K/mol, and the paramagnetic Curie temperature (Weiss constant) $\theta_P = 19.4$ K. This value is slightly higher than the temperature of the ferromagnetic transition $T_{FM} \approx 19$ K that we extracted from the low temperature magnetization experiments. From the obtained Curie-Weiss constant C, the effective moment per formula unit (f.u.) can be estimated as $P_{\rm eff} \simeq 9.1\ \mu_B$/f.u., which is larger than the expected value of $g\sqrt{S(S+1)}\mu_B = 7.94\ \mu_B$ for a free Eu^{2+} ion with $S = 7/2$ and $g = 2$. This deviation may be caused by the ferromagnetic Fe_2P impurity, mentioned previously. The positive value of θ_P is indicative of ferromagnetic interactions between Eu^{2+} spins along the c-axis. Flat $\chi_c(T)$ below θ_P is typical for ferromagnets with formation of antiparallel domains along the c-axis.

Section S2. Interplay between superconductivity and ferromagnetism in $EuFe_2(As_{0.79}P_{0.21})_2$: Supplementary MFM maps

In addition to the Fig. 3 of the main manuscript the following figures fig. S3 and fig. S4 give additional details to the formation of DMS, spontaneous vortex phase and DVS structure upon cooling.

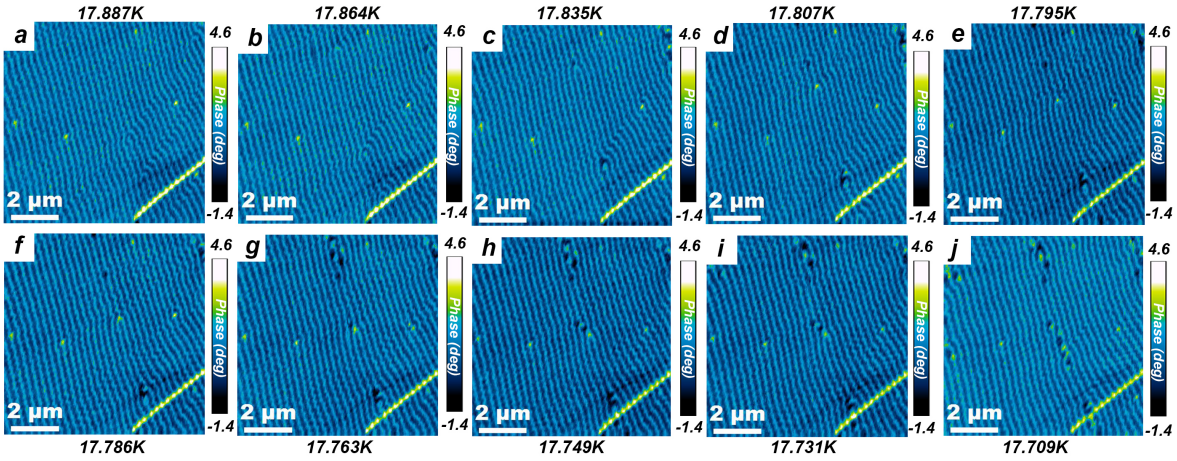

Fig. S3. Full set of images of spontaneous V-AV generation. a-j - magnetic MFM maps acquired in the temperature window $\Delta T \approx 0.18$ K from $T = 17.887$ K (a) to $T = 17.709$ K (r) in the same sample area $8\ \mu$m $\times 8\ \mu$m as in Fig. 3 of the main text.

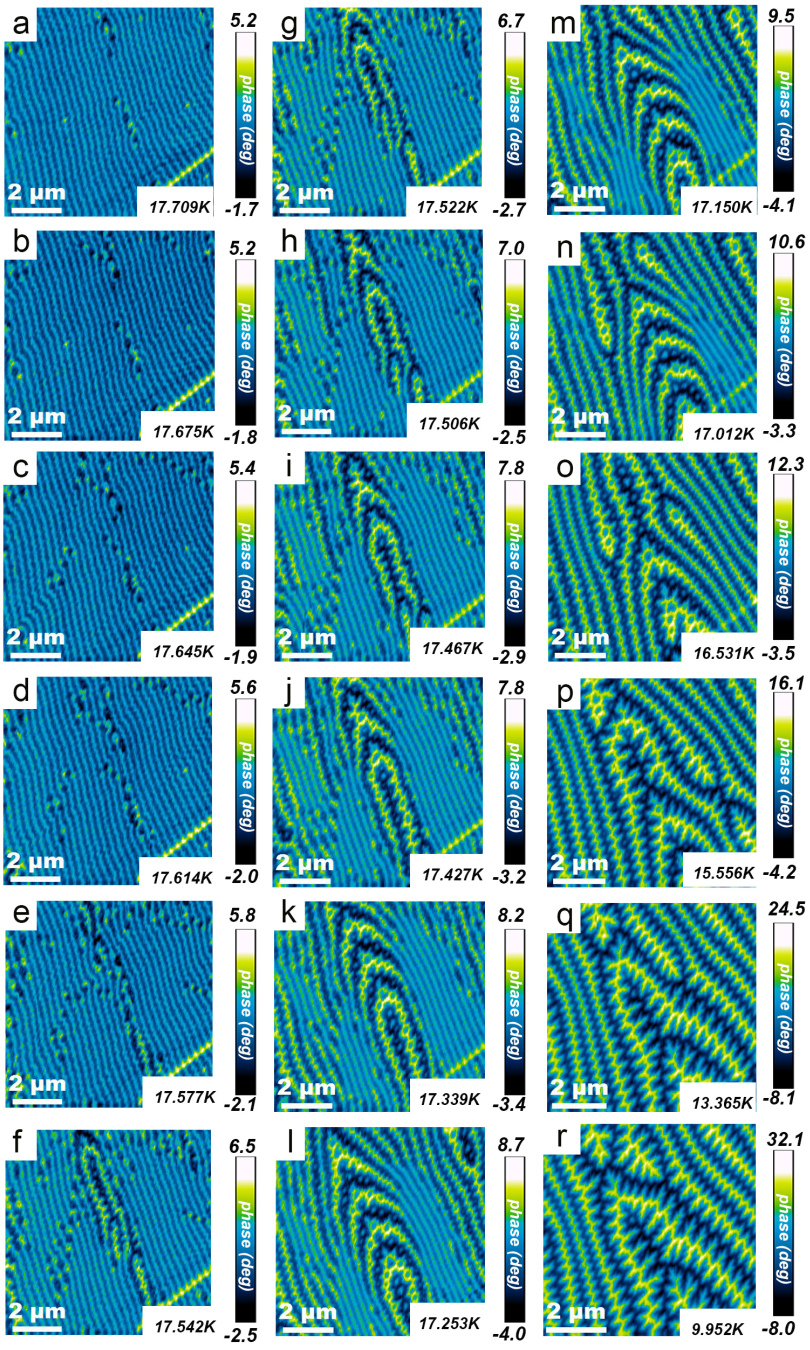

Fig. S4. Full set of maps demonstrating the domain structure evolution at DMS/DVS transition. a-i - magnetic MFM maps acquired from $T = 17.709$ K (a) to $T = 9.252$ K (k) in the same sample area 8 μm $\times$8 μm as in Fig. 3 of the main text.

Section S3. Energy balance between FM and SC states

In $EuFe_2(As_{0.79}P_{0.21})_2$ the DMS is realized in a narrow temperature range 17.864 - 18.234 K. Inside the DMS the domain width l evolves smoothly with temperature yet it remains much shorter than both the sample thickness d_F $\sim$12 μm and the penetration depth $\lambda(0) \sim 350$ nm (*33-35*). The smooth temperature evolution of l is a result of a competition between a weak FM order and SC screening in the DMS. In non-SC ferromagnets the equilibrium domain width l_N originates from the balance between the energy term related to the magnetic induction (stray field energy) which tends to create alternating FM domains and thus reduce l, and the energy cost of the domain walls $M^2\widetilde{w}d_F/l$ per unit surface, where M and $\widetilde{w}$ are respectively the magnetization and the effective width of the domain wall, and $M^2\widetilde{w}$ is the specific wall energy (*18*). As a result, in non-superconducting FM materials the domains form a quasi-periodic domain structure, usually in a few microns range, related to the sample thickness d_F. In our case, however, the FM subsystem is magnetically coupled to the SC one, that makes the energy balance more subtle. When $l << l_N$ the ferromagnetism tends to increase $l \to l_N$, thus reducing the density of domain walls and corresponding energy contribution, while the kinetic energy of Meissner currents which are spontaneously generated to screen the rising magnetic field in alternating up- and down- domains and the stray field energy increase with l (*19*). Precise calculations show (*16*) that the energy E_{DMS} of the DMS in thin ferromagnetic superconductor depends on the domain width l as

$$E_{DMS} = M^2\frac{l_N^2}{\lambda}\left\{2\Lambda^2 L\pi\left[1-\frac{2}{\pi\widetilde{l}}\tanh\left(\frac{\pi\widetilde{l}}{2}\right)\right]+\frac{32\widetilde{l}\Lambda^2}{\pi}\sum_{k=0}^{\infty}\frac{2k+1}{\left[\widetilde{l}^2+(2k+1)^2\right]^{3/2}\left[2k+1+\sqrt{\widetilde{l}^2+(2k+1)^2}\right]}\right.$$
$$\left.+\frac{14\varsigma(3)}{\pi^3}\frac{1}{\widetilde{l}}\right\}$$

where $\widetilde{l}$ is the dimensionless domain width in the DMS, $\widetilde{l} = \frac{l}{\pi\lambda}$, l_N is the width of the intrinsic domains of the same FM material in the absence of superconductivity, $l_N = \sqrt{d_F\widetilde{w}\pi^2/14\varsigma(3)}$, $\varsigma(3) =$

1.202, and the normalized lengths, $\Lambda = \frac{\lambda}{l_N}$, $L = \frac{d_F}{\lambda}$. The last term is the contribution of the domain wall energy $M^2\widetilde{w}$, which is assumed to be the same in the Meissner and normal states. Owing to the Meissner currents the energy of the inherent DMS phase is obviously larger than the energy E_{FM} of the FM domain structure in the absence of superconductivity. E_{FM} can be obtained from the expression for E_{DMS} in the limit $\lambda \to \infty$

$$E_{FM}(l) = M^2 \frac{14\varsigma(3)}{\pi^2}\left[l + \frac{l_N^2}{l}\right]$$
$$E_{FM}^{\min} = M^2 \frac{28\varsigma(3)}{\pi^2} l_N$$

For calculation of l_{DMS} and l_N we consider the normalized energy of domain structure $\widetilde{E}_{DMS}(\widetilde{E}_{FM}) = E_{DMS}(E_{FM})\frac{\lambda}{M^2 l_N^2}$ in the Meissner and (normal) states, respectively. Also, according to Ref. (*36*) for ferromagnetic superconductor in the vortex state when $4\pi M_{\rm s} \gg H_{\rm c1}$ and $d_F \gg l_N$ the period of domain structure is basically the same as in the normal phase, and therefore we assume $l_N = l_{DVS}$. The curves $\widetilde{E}_{DMS}(\widetilde{l})$ and $\widetilde{E}_{FM}(\widetilde{l})$ are presented in fig. S5. The equilibrium domain width $\widetilde{l}$ corresponds to the minimum of $\widetilde{E}_{DMS}(\widetilde{l})$ (see fig. S5). With $d_F = 12$ μm, $T = 18$ K and $\lambda(18\ K)$ =420 nm it gives $l \approx 137$ nm - in a good agreement with the experiment. Notice that l evolves with temperature since $\lambda(T)$; also l_N is temperature dependent, as discussed in the main text.

When the temperature is decreased below T_{FM}, the local magnetization M increases. Both μSR and neutron diffraction experiments made on $EuFe_2(As_{1-x}P_x)_2$ single crystals with $x = 0.19$ show that the saturation magnetization just below T_{FM} increases rather fast

$$M(T) = M(0)(1 - T/T_{FM})^{\delta}$$

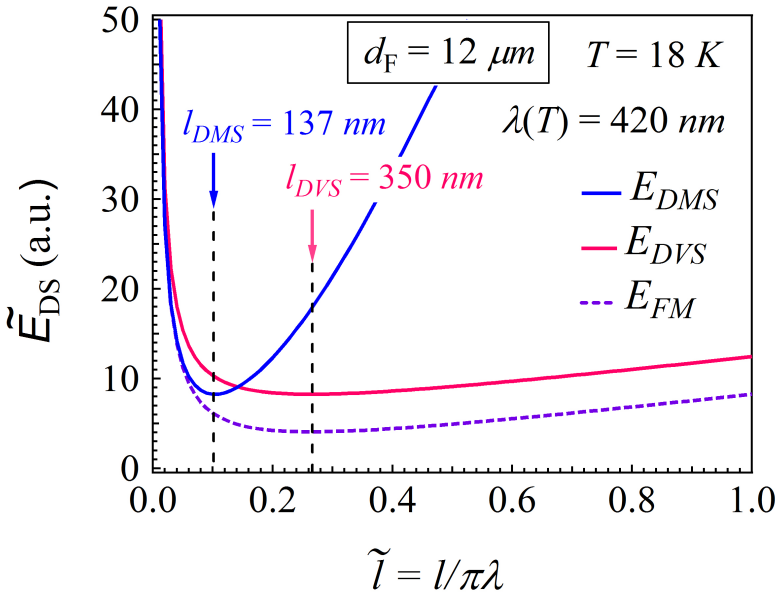

Fig. S5. The total energy of the domain structure $\tilde{E}_{DS}$ in the Meissner and normal states. The total energy of the domain structure $\widetilde{E}_{DS}$ in the Meissner and normal states as a function of the normalized domain width $\widetilde{l}$. The minimum energy is obtained for $l_{DMS} \sim 137$ nm, in agreement with the experiment.

with the exponent $\delta \sim 0.36$ (*32, 37,38*).This increases the energy of the Meissner currents and raises E_{DVS}. When $\widetilde{E}_{DMS}$ reaches $\widetilde{E}_{DVS}$, $\widetilde{E}^{\min}_{DVS} = \widetilde{E}^{\min}_{DMS}$, the first-order phase transition from DMS to DVS takes place, accompanied by a sudden jump of the period. Notice that the presence of vortices and antivortices only slightly increases the energy of the domain structure, as compared with a non-superconducting ferromagnetic case (*23*)

$$E_{DVS}(l) \simeq E_{FM}(l) + MH_{c1}d_F$$

From the Fig. 2(b) we see that the transition to DVS phase should occur at $\frac{H_{c1}d_F\lambda}{Ml_N^2} \approx 4.17$.

With $\lambda_{ab}(\sim T_{FM}) \sim 420$ nm, $l_N \sim l_{DVS} = 350$ nm, $\xi_{ab}(\sim T_{FM}) \sim 9.1$ nm, $\kappa = \lambda_{ab}/\xi_{ab} \sim 46$, and estimated $H_{c1}(\sim T_{FM}) = 40.4$ Oe along the c axis, the magnetization at the transition from DMS to DVS, $M_c \approx \frac{H_{c1}d_F\lambda}{4.17l_N^2} \approx 398.9$ G, and $B_c = 4\pi M_c \approx 5$ kG (thus $B_c >> H_{c1}$). Notice that the minimum

for the total energy of DVS/FM is very shallow compared to that of DMS. This could explain why the DVS pattern is more developed and less regular than the DMS one.

In $EuFe_2(As_{0.79}P_{0.21})_2$ the internal magnetic field at low temperatures $B_{in}(T << T_{FM}) = 4\pi M(0) \approx 9$ kG (*6*), and then we can roughly estimate the temperature T_1 of the transition from DMS to DVS as

$$\frac{T_{FM} - T_1}{T_{FM}} \sim \left(\frac{B_c}{B_{in}(0)}\right)^{1/\delta} \sim 1.97 \cdot 10^{-1}$$

For $T_{FM} = 18.2$ K, we find $T_{FM} - T_1 \sim 3.583$ K, in a qualitative agreement with the experiment.

Following the results of Dao *et al.* (*17*) and Khaymovich *et al.* (*36*) we can also estimate the threshold magnetization M_{th} for the transition between DMS and DVS. According to Ref. (*17*) at $M > M_{th}$, the energy for the creation of a vortex-antivortex (V-AV) pair in the middle of adjacent domains becomes negative. If we assume that the pinning energy for vortices and domain walls and the Bean-Livingston barrier are small at T_1 , the magnetization threshold for narrow domains $l \ll d_F$, and for $l \ll \lambda$ takes the form

$$4\pi M_{th} = \frac{2\Phi_0 \ln(l/\xi)}{\pi l^2}, l \ll d_F, \lambda$$

One can see from the expression for M_{th} that the intervortex distance within ferromagnetic domains at DMS-DVS transition is comparable to the domain width l, and for $l \ll \lambda$ the internal magnetic field $4\pi M_{th}$ needed for generation of V-AV pairs is much larger than H_{c1}.

For the average $l_{DMS} = 137$ nm, the transition to DVS occurs at the magnetization threshold $M_{th} \approx 152$ G and corresponding internal magnetic field $B_{th} = 4\pi M_{th} \approx 1.91$ kG (still $>> H_{c1}$). Using the above presented temperature dependence of the magnetization $M(T)$ (*37*) and the known value for $B_{in}(T << T_{FM})$ (*6*), we can have an alternative estimate for T_1

$$\frac{T_{FM} - T_1}{T_{FM}} \sim \left(\frac{B_{th}}{B_{in}(0)} \right)^{1/\delta} \sim 1.4 \cdot 10^{-2}$$

For $T_{FM} = 18.2$ K, we find $T_{FM} - T_1 \sim 0.259$ K.

Finally, the agreement between the theory and experiment is very good both in the determination of the Meissner domain width and the temperature of the DMS-DVS transition.

Section S4. Simultaneous V-AV nucleation at FM domain boundaries

When the temperature is lowered below the FM transition the striped DMS phase is realized (see Fig. 1e of the main manuscript, the schematic view is presented in fig. S6(A)). Since the neighbouring FM domains have opposite magnetic orientations, the circulation of the Meissner currents is also alternating: they circulate either clockwise or counterclockwise in the plane perpendicular to the magnetization vector. Consequently, the Meissner currents flow in the same direction on both sides of the same domain wall and reinforce each other. By symmetry, they also cancel each other in the central parts of the domains (black dashed lines in fig. S6 represent zero-current lines). When the temperature is further lowered, the magnetization of the FM domains increases, and the kinetic energy of screening Meissner currents rises. The kinetic energy density is maximum near domain walls where the current density is strongest. As a result, the SC order near domain walls is weakened, facilitating vortex-antivortex (V-AV) core nucleation. That is the reason why the nucleation of a V-AV pairs takes place at the domain walls. Additional local defects (trapped Abrikosov vortices, domain structure defects, already existing vortices and antivortices etc.) which also deplete the SC order parameter play role of local nucleation centres.

At the initial stage of nucleation the cores of the V-AV pairs are generated (fig. S6(B)). The energy cost of this nucleation is rather low as the SC order at the domain walls and defects is weak. By the same reason the vortex (antivortex) currents which circulate around the vortex core with 2π (-2π) phase singularity are not strong. As a result the total currents are not redistributed significantly. Since at this stage the cores of the vortex and antivortex are very close to each other ($<< \lambda$) the magnetic flux due to the nucleation of the V-AV pair is almost zero; it is undetectable in the MFM maps. When vortex and antivortex separate and enter the respective up- and down- FM domains, where the SC order parameter is higher, the vortex currents circulating around the cores increase. In each FM domain the vortex (antivortex) currents circulate in the direction opposite to the Meissner currents. Therefore the vortex (antivortex) currents partially compensate the Meissner ones and locally reduce the kintetic energy

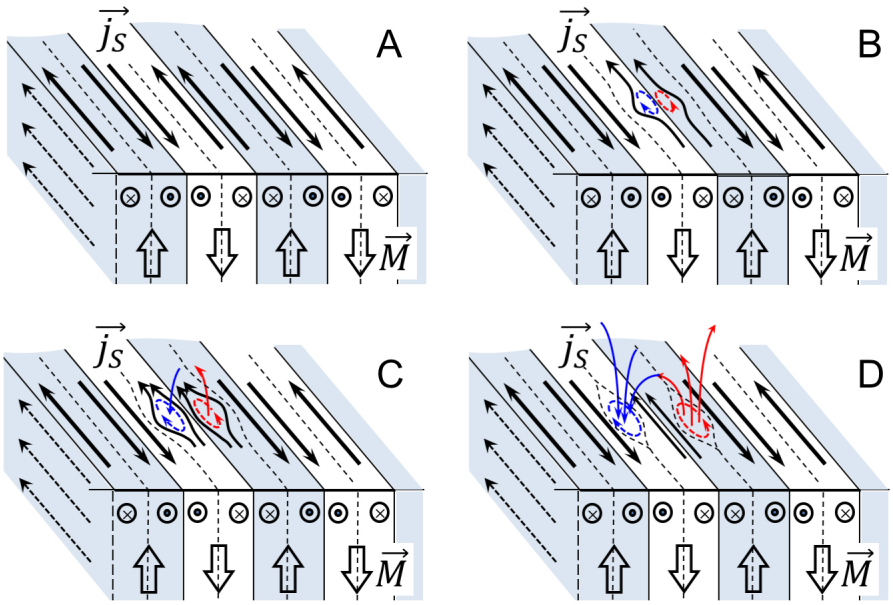

Fig. S6. Schematics of the local V-AV nucleation.

Schematics of the local Vortex - Antivortex nucleation in $EuFe_2(As_{0.79}P_{0.21})_2$. A - Schematic view on Meissner current flow in the DMS phase, the Meissner currents (marked by black arrows). In each domain the currents are strong near domain walls. They circulate in the same direction on both sides of domain walls and cancel each other in the central parts of the domains (black dashed lines represent zero-current lines). B - nucleation of a vortex-antivortex (V-AV) pair at the domain wall. At the beginning stage only the two V-AV cores are generated (not to scale: the cores nucleate on the scale of the SC coherence length, $\xi \simeq 9\,\mathrm{nm}$ (at $T \sim T_{FM}$, see above). The initial distribution of currents is not affected significantly, as the order parameter near domain walls is reduced. Since the cores of the vortex and antivortex are very close to each other ($<< \lambda$) the magnetic flux due to the nucleation of the V-AV pair is almost zero. C - penetration of vortex and antivortex in the neighbouring domains of opposite magnetization. The vortex currents partially compensate the Meissner ones thus reducing the kintetic energy density. As the V-AV cores get spatially separated a non-zero magnetic flux appears. D - in DVS phase the vortices and antivortices partially relax magnetic and kinetic energy terms.

density. The magnetic screening is also reduced, thus partially relaxing the magnetic energy.

When the V-AV cores get spatially separated a non-zero magnetic flux appears. This flux is detected in MFM experiment as tiny neighbouring white and black spots (fig. S6(C)). Deep in the DVS phase vortices and antivortices enable relaxing the magnetic energy and reducing the kinetic energy of currents. Notice that since the vortex-antivortex separation is $\lesssim \lambda$ none of this quantum objects carry full flux quantum.